2010

Charge transport in dye-sensitized solar cells based on flame-made TiO2 nanoparticles

George Tsekouras
University of Wollongong

Masanori Miyashita
Shinshu University

Yung Kent Kho
University of New South Wales

Wey Yang Teoh
University of New South Wales

Attila J. Mozer
University of Wollongong, attila@uow.edu.au

See next page for additional authors

Charge transport in dye-sensitized solar cells based on flame-made TiO2 nanoparticles

Abstract

The fundamental understanding on charge-transport properties of flame-synthesized TiO2 in dye-sensitized solar cells (DSSCs) is established in this work. By employing a one-step flame spray pyrolysis (FSP), predominantly anatase TiO2 nanoparticles with average nanoparticle sizes between 11 and 36 nm were achieved by varying the rate of combustion enthalpy (through varying liquid precursor feed flow rates) and using either an “openflame” or “enclosed-flame” configuration. Electron diffusion coefficient (D), electron lifetime (τ), open circuit voltage (Voc), and capacitance (C) measurements carried out on FSP TiO2 -based DSSCs demonstrated that interband charge trap density decreased with increase in particle size. Compared to earlier studies, interband charge trap density could be controlled more independently of particle size. Under one-sun conditions, relatively high Voc was measured with large particle size due to the lowering of interband charge trap density. This was true despite the associated shorter τ . Comparisons with commercial benchmark Nanoxide-T and Degussa P25 TiO2 were also carried out. The results from the current study have significant implications on the design of TiO2 nanoparticles by flame aerosol techniques, for DSSCs as well as other photoelectrochemical applications. Index Terms—Electron diffusion coefficient

Disciplines

Life Sciences | Physical Sciences and Mathematics | Social and Behavioral Sciences

Publication Details

Tsekouras, G., Miyashita, M., Kho, Y., Teoh, W., Mozer, A. J., Amal, R., Mori, S. & Wallace, G. G. (2010). Charge transport in dye-sensitized solar cells based on flame-made TiO2 nanoparticles. IEEE Journal on Selected Topics in Quantum Electronics, 16 (6), 1641-1648.

Authors

George Tsekouras, Masanori Miyashita, Yung Kent Kho, Wey Yang Teoh, Attila J. Mozer, Rose Amal, Shogo Mori, and Gordon G. Wallace

Charge Transport in Dye-Sensitized Solar Cells Based on Flame-made TiO_2 Nanoparticles

George Tsekouras, Masanori Miyashita, Yung Kent Kho, Wey Yang Teoh, Attila Janos Mozer, Rose Amal, Shogo Mori, and Gordon G. Wallace

***Abstract*—The fundamental understanding on charge-transport properties of flame-synthesized TiO_2 in dye-sensitized solar cells (DSSCs) is established in this work. By employing a one-step flame spray pyrolysis (FSP), predominantly anatase TiO_2 nanoparticles with average nanoparticle sizes between 11 and 36 nm were achieved by varying the rate of combustion enthalpy (through varying liquid precursor feed flow rates) and using either an "open-flame" or "enclosed-flame" configuration. Electron diffusion coefficient (D), electron lifetime (τ), open circuit voltage (V_{oc}), and capacitance (C) measurements carried out on FSP TiO_2-based DSSCs demonstrated that interband charge trap density decreased with increase in particle size. Compared to earlier studies, interband charge trap density could be controlled more independently of particle size. Under one-sun conditions, relatively high V_{oc} was measured with large particle size due to the lowering of interband charge trap density. This was true despite the associated shorter τ. Comparisons with commercial benchmark Nanoxide-T and Degussa P25 TiO_2 were also carried out. The results from the current study have significant implications on the design of TiO_2 nanoparticles by flame aerosol techniques, for DSSCs as well as other photoelectrochemical applications.**

***Index Terms*—Electron diffusion coefficient (D), electron lifetime, flame spray pyrolysis (FSP), nanoparticle.**

I. Introduction

DYE-SENSITIZED solar cells (DSSCs) based on mesoporous TiO_2 have been subjected to extensive scientific and commercial interest ever since the report on such device by O'Regan and Grätzel [1]. This is well in line with the increasing global demand for clean and renewable energy, where DSSCs may potentially offer an economical solution to solar-to-electrical energy conversion. Upon photoirradiation, surface-bound dye molecules are excited and inject electrons into the TiO_2 conduction band. The electrons are channeled through an external circuit to the counter electrode, where the I_3^-/I^- redox couple completes the electrons cycle by quenching the photooxidized dye. Despite its conceptual elegance and simplicity, the operation of DSSCs involves a multitude of intricate processes originating in the TiO_2 photoanode, such as interparticle charge transport, percolation of electrons, charge trapping, and recombination. Hence, it is not surprising that the structural and physicochemical characteristics of the TiO_2 photoanode impart a critical influence on the overall DSSC performance.

To date, the best performing TiO_2 optimized for DSSC applications is made by a multistep hydrothermal method, yielding highly crystalline faceted nanoparticles, and a champion DSSC of 11.4% power conversion efficiency [2]. The hydrothermal preparation conditions impart significant influence on the charge transport and recombinations [3]. While the flame synthesis of TiO_2 is known for its rapid (milliseconds) and high-throughput synthesis, yielding also highly crystalline nanoparticles, its applications for DSSCs have been largely limited to the commercial Degussa P25 (maximum reported efficiency of around 9%) [4]. The lack of variations in commercial flame-made TiO_2 samples other than the standard P25 material renders their assessment and more importantly their charge transport poorly understood. With increasing interest in the flame synthesis of nanomaterials in recent years [5], the exclusivity of such technique is becoming a thing of the past. More specifically, the variability in the physicochemical properties of TiO_2 during flame synthesis, resulting in the tuning of its photocatalytic behavior, has been extensively studied by us [6]–[9] as well as others.

In the current study, we establish the relationship between the characteristics of flame-made TiO_2 and its charge transport and photovoltaic behavior in DSSCs. Direct manipulation of the TiO_2 nanoparticle surface area and defect contents (through a series of parametric modifications of the flame synthesis) has pronounced effects on charge-transport properties. To the best of our knowledge, this study is the first to report systematically on the effect of TiO_2 flame synthesis on the fundamental charge transport in these materials, and specifically assessed in relation to their performance as DSSCs. This fundamental knowledge is of importance also to other photoelectrochemical applications, such as photo-assisted water splitting and photocatalysis.

Manuscript received March 9, 2010; revised April 12, 2010; accepted April 27, 2010. Date of publication July 12, 2010; date of current version December 3, 2010. This study was supported by the Center of Excellence program, Australian Research Council.

G. Tsekouras was with the Australian Research Council Center of Excellence for Electromaterials Science, Intelligent Polymer Research Institute, University of Wollongong, Fairy Meadow, N.S.W. 2519, Australia. He is now with the University of St Andrews, Fife, KY16 9ST, U.K.

M. Miyashita was with the Department of Fine Materials Engineering, Shinshu University, Ueda, Nagano 386-8567, Japan. He is now with Toray Industries, Inc., Tokyo 103-8666, Japan.

Y. K. Kho and R. Amal are with the Australian Research Council Center of Excellence for Functional Nanomaterials, School of Chemical Sciences and Engineering, The University of New South Wales, Sydney, N.S.W. 2052, Australia.

W. Y. Teoh was with the Australian Research Council Center of Excellence for Functional Nanomaterials, School of Chemical Sciences and Engineering, The University of New South Wales, Sydney, N.S.W. 2052, Australia. He is now with the City University of Hong Kong, Kowloon, Hong Kong.

A. J. Mozer and G. G. Wallace are with the Australian Research Council Center of Excellence for Electromaterials Science, Intelligent Polymer Research Institute, University of Wollongong, Fairy Meadow, N.S.W. 2519, Australia (e-mail: attila@uow.edu.au; gordon_wallace@uow.edu.au).

S. Mori is with the Department of Fine Materials Engineering, Shinshu University, Ueda, Nagano 386-8567, Japan.

Digital Object Identifier 10.1109/JSTQE.2010.2049734

II. Experimental

A. Flame Synthesis of TiO_2 Nanoparticles and Photoanode Fabrication

The liquid precursor for the synthesis of TiO_2 nanoparticles via flame spray pyrolysis (FSP) has been described earlier [9]. Briefly, a liquid precursor consisting of 0.65 M Ti was prepared by mixing titanium (IV) tetraisopropoxide (TTIP), xylene, and CH_3CN in the volume ratio 20:55:25, respectively. During FSP, the liquid precursor was delivered to the flame nozzle [9] at a controlled flow rate (3, 5, or 7 mL·min^{-1}) using a syringe pump (Inotech R232). At the nozzle tip, the liquid precursor was atomized by the dispersant O_2 (1.5 bar) and simultaneously ignited by a surrounding supporting oxymethane flame (3.2 L·min^{-1} O_2 and 1.5 L·min^{-1} CH_4). A 5 L·min^{-1} sheath of O_2 was issued through the outer most ring. This configuration is termed "open-flame," since the FSP was exposed to ambient air. For the "enclosed-flame" configuration, the FSP was enclosed in a quartz tube (outer diameter = 7 cm, l = 50 cm) to prevent entrainment of the ambient air as well as to preserve convective heat. The temperature within the tube was controlled by issuing 40 L·min^{-1} of O_2 or N_2–O_2 mixture. Aerosol TiO_2 powders were collected on a glass fiber filter (Whatmann GF/D) with the aid of a vacuum pump (Alcatel SD series).

As-prepared FSP TiO_2 powders were formulated into pastes by suspending 0.8 g TiO_2 in 8 g ethanol (EtOH) and sonicating using a Branson sonic probe for 20 min. Thereafter, 0.22 g ethyl cellulose and 3.0 g of terpineol were added stepwise with the mixture sonicated for 1 min after each addition. The mixture was stirred and heated in a 70–80 °C water bath to evaporate EtOH. A consistent final paste was achieved following 10 min of milling in a three-roll mill. In the case of commercial P25 powder, the paste was prepared in distilled water as described elsewhere [10]. The TiO_2 pastes (FSP, P25 and Solaronix Ti-Nanoxide T/SP) were doctor-bladed onto SnO_2:F (FTO)-coated glass and sintered at 500 °C for 30 min in air. The area and thickness of calcined TiO_2 films was ~0.17 cm^2 and 5–6 μm, respectively. Sensitization was achieved by placing transparent sintered films at ~110 °C in a 0.3 mM solution of Ru sensitizer dye N719 (Peccell Technology) in 1:1 (by volume) CH_3CN:t-butyl alcohol and left overnight at room temperature.

B. TiO_2 Powder and Film Characterization

X-ray diffraction (XRD) of TiO_2 powders was carried out on a Philips X'Pert MPD equipped with a pixel array detector, operating at 40 kV, 40 mA with 2θ (Cu Kα) = 20°–70°, step size = 0.02°. XRD spectra of TiO_2 films were collected on a Philips X'Pert MRD diffractometer operating at 40 kV, 40 mA with 2θ (Cu Kα) = 20°–70°, step size = 0.02°. The crystallite size and phase compositions of powders and films were estimated by the Rietveld method [11] using X'Pert Highscore Plus software. Specific surface areas (SSAs) of powders and films were estimated from N_2 adsorption–desorption isotherm at 77 K on a Micromeritics Tristar 3000. High resolution TEMs were obtained using a Philips CM200 TEM operating at 200 kV. Surface morphology of TiO_2 films was analyzed on a Hitachi S900 field-emission SEM. Film thicknesses were measured using a Dektak surface profilometer.

C. Dye-Sensitized Solar Cell Assembly and Testing

Dye-sensitized mesoporous TiO_2 photoanodes were sandwiched with Pt counter electrodes. The liquid electrolyte contained 0.6 M 2,3-dimethyl-1-propylimidazolium iodide, 0.05 M I_2, 0.1 M LiI, and 0.5 M t-butyl pyridine in CH_3CN. *I–V* characteristics of DSSCs were measured on a Solar Simulator under AM1.5 and 100 mW·cm^{-2} illumination intensity (YSS-100 A, Yamashita Denso) without an aperture mask.

D. Electron Diffusion Coefficient (D), Electron Lifetime (τ), Open-Circuit Voltage (V_{oc}), and Capacitance (C) Measurements

The DSSCs used for D, τ, V_{oc}, and C measurements were the same as those used for *I–V* characterization. Measurements were achieved using the stepped light-induced transient measurements of photocurrent and voltage (SLIM-PCV) technique, as described elsewhere [12]. In short, a continuous laser (Lablaser, Coherent, λ = 635 nm) was irradiated over the entire area of DSSCs, and a small portion of the laser intensity was stepped down. Then, induced current transients at short-circuit, and voltage transients at open circuit, were recorded by a fast multimeter (Advantest, AD7461 A). The transients were fitted with a single exponential function whereupon D and τ were obtained. Electron density in DSSCs was obtained by an earlier described charge-extraction method [13], [14]. Note that the porosity of the electrode, which would be expected to be between ~50–60% [3], [15], was not taken into account in order to calculate electron density. Capacitance was measured by an earlier reported method using a pulsed laser illumination superimposed on a bias light [16], [17]. First, the amount of charge photogenerated by a pulse was measured, and then the V_{oc} increase by the same pulse was determined under various bias light intensities. The amount of photogenerated charge was divided by the V_{oc} increase to give C, described as per unit of projected area. All measurements were repeated under various laser intensities and with two identical DSSCs.

III. Results and Discussion

A. Flame Synthesis of TiO_2 Nanoparticles and Photoanode Fabrication

Pristine TiO_2 nanoparticles with controllable SSAs were synthesized via single step FSP. Here, variation in the rate of combustion enthalpy was carried out by controlling the flow rates of the liquid precursor, consisting of TTIP in xylene/CH_3CN, to the FSP nozzle. Typically, combustion of the liquid spray droplets ($\Delta H_{combustion} = -31.7$ kJ·mL^{-1}) results in a high temperature flame of $T_{max} \sim 2800$ K [18], within which TiO_2 nanoparticles are formed via the gas-to-particle route [19]. Continuous and rapid heat loss through radiation and ambient air entrainment further give rise to a steep temperature gradient (~170 K·cm^{-1}) along the flame axis [18], allowing supersaturation of Ti vapor to form fine nuclei and subsequent particle growth by coalescence, aggregation, and agglomeration. Following this path

TABLE I
PROPERTIES OF FSP AND COMMERCIAL TiO_2 POWDERS AND THE CORRESPONDING FABRICATED TiO_2 FILMS

	Powder				Film			
TiO_2	d_A[a] (nm)	d_R[a] (nm)	X_A[b] (wt.%)	SSA[c] ($m^2\ g^{-1}$)	d_A[a] (nm)	d_R[a] (nm)	X_A[b] (wt.%)	SSA[c] ($m^2\ g^{-1}$)
FSP-1	11	3	82	134	12	5	91	82
FSP-2	15	4	86	89	15	6	91	66
FSP-3	18	7	84	71	19	7	93	55
FSP-4[e]	32	28	82	23	32	28	82	21
FSP-5[e]	36	28	88	22	35	30	88	19
Nanoxide-T	13	-	100	120[d]	21	-	100	62
P25	20	28	74	50	21	27	78	41

[a] d_A = average anatase and d_R = average rutile crystallite sizes determined from XRD spectra using Rietveld analysis and Scherrer equation.
[b] X_A = anatase mass fraction, determined by Rietveld analysis.
[c] SSA = specific surface area obtained from Brunauer-Emmet-Teller (BET) measurements.
[d] Manufacturer's claims.
[e] Particles synthesised in an enclosed-flame configuration.

of formation, TiO_2 nanoparticles designated FSP-1, FSP-2, and FSP-3 with SSA values of 134, 89, and 71 $m^2 \cdot g^{-1}$ (see Table I) were synthesized via the "open-flame" configuration, where the flame was exposed to ambient atmosphere, at liquid feed flow rates of 3, 5, and 7 $mL \cdot min^{-1}$, respectively. The resultant TiO_2 nanoparticles were highly crystalline as evident from the XRD spectra (see Fig. 1), as well as the clear lattice fringes observed in the high resolution transmission electron microscope images in Fig. 2. The spherical particles consisted of predominantly anatase fraction ($X_A = 82$–86 wt%, Table I), in agreement with the general synthesis of TiO_2 nanoparticles by FSP [9], [18], [20].

In a modified configuration, the FSP was enclosed in a quartz tube, hereby referred to as "enclosed-flame" [21]. Enclosure by the quartz tube restricts ambient air entrainment, thereby prolonging the flame residence time and the zone of high temperature [20]. As such, a higher degree of aerosol sintering could take place resulting in larger particles (i.e., lower SSA). Synthesis of TiO_2 in the enclosed configuration at precursor feed flow rates of 5 and 7 $mL \cdot min^{-1}$ yielded particles with similarly low SSA values of 23 and 22 $m^2 \cdot g^{-1}$ and anatase fractions of 82 and 88 wt%, respectively (see Table I). These samples are hereafter designated FSP-4 and FSP-5, respectively. The small difference in SSA between these two samples, despite different rates of combustion enthalpy, showed that rapid quenching was successfully impeded using the enclosed-flame method, resulting in similar flame temperature–time profiles. In addition to displaying sharp lattice fringes, the resultant particles were also faceted [see Fig. 3(a) and (b)], bearing qualitative morphological resemblance to P25 [see Fig. 3(c)] and Nanoxide-T [see Fig. 3(d)].

Mesoporous particulate films were prepared from the FSP TiO_2 samples as well as P25 and Nanoxide-T (see Fig. 4). Despite the high temperature calcination at 500 °C encountered during film fabrication, the particles preserved their crystallite sizes, with the exception of Nanoxide-T (see Table I and Fig. 5). The hydrothermal preparation of Nanoxide-T and associated much lower synthesis temperature compared to flame techniques resulted in lower thermal stability. While the anatase content of sintered films did not vary significantly with respect to their powder forms, FSP TiO_2 films did show a trend of decreasing SSA as a function of initial SSA (i.e., powder). The decrease varied from 134 to 82 $m^2 \cdot g^{-1}$ for FSP-1

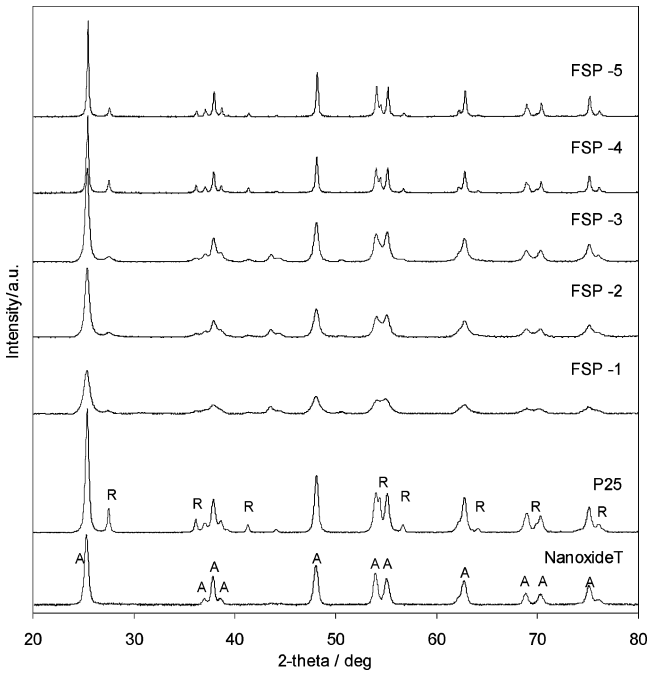

Fig. 1. XRD spectra of As-prepared FSP TiO_2 powder samples as well as Degussa P25 and Nanoxide-T. The characteristics peaks of anatase are labeled "A", while those of rutile are labeled "R".

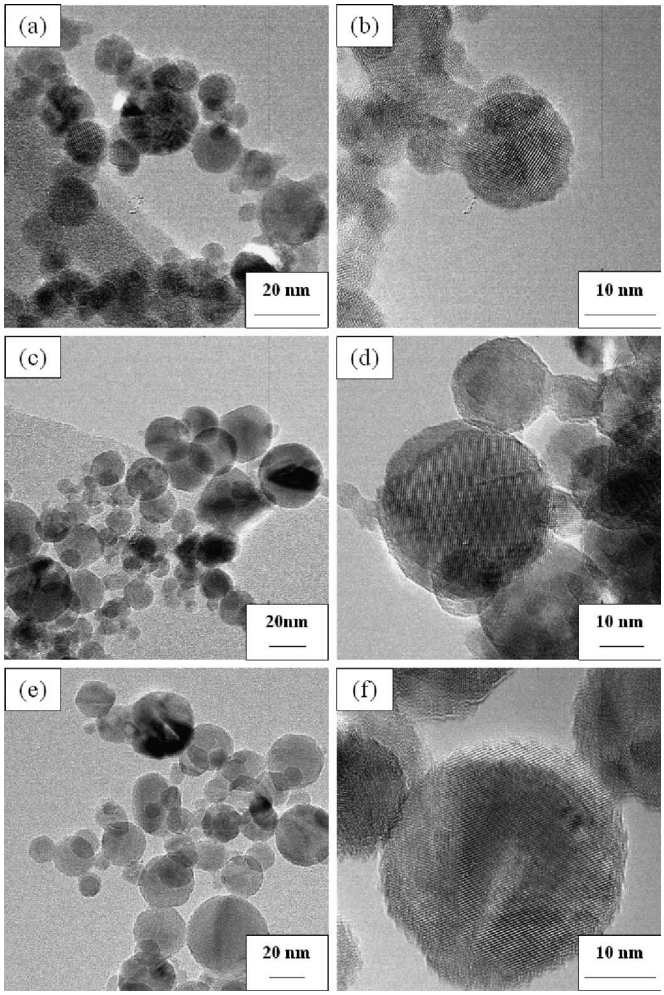

Fig. 2. TEM images of TiO_2 nanoparticles As-prepared in the open-flame configuration. (a) and (b) FSP-1, (c) and (d) FSP-2, (e) and (f) FSP-3.

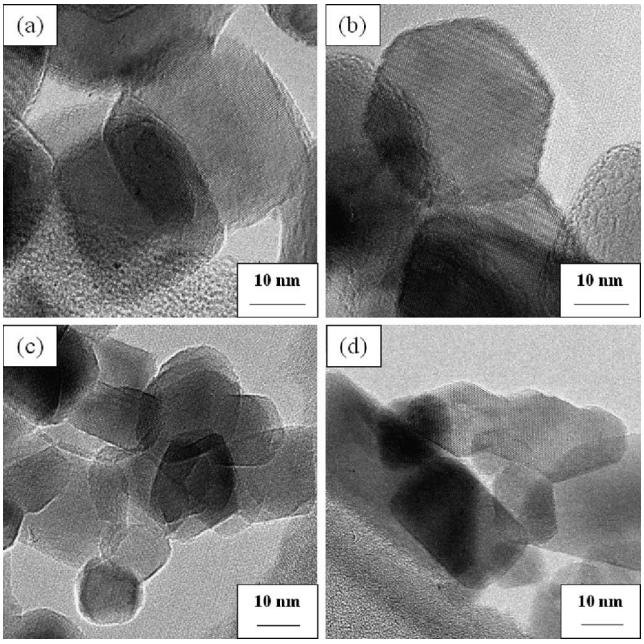

Fig. 3. TEM images of TiO_2 nanoparticles As-prepared in the enclosed-flame configuration. (a) FSP-4, (b) FSP-5, as well as commercial (c) P25 and (d) Nanoxide-T.

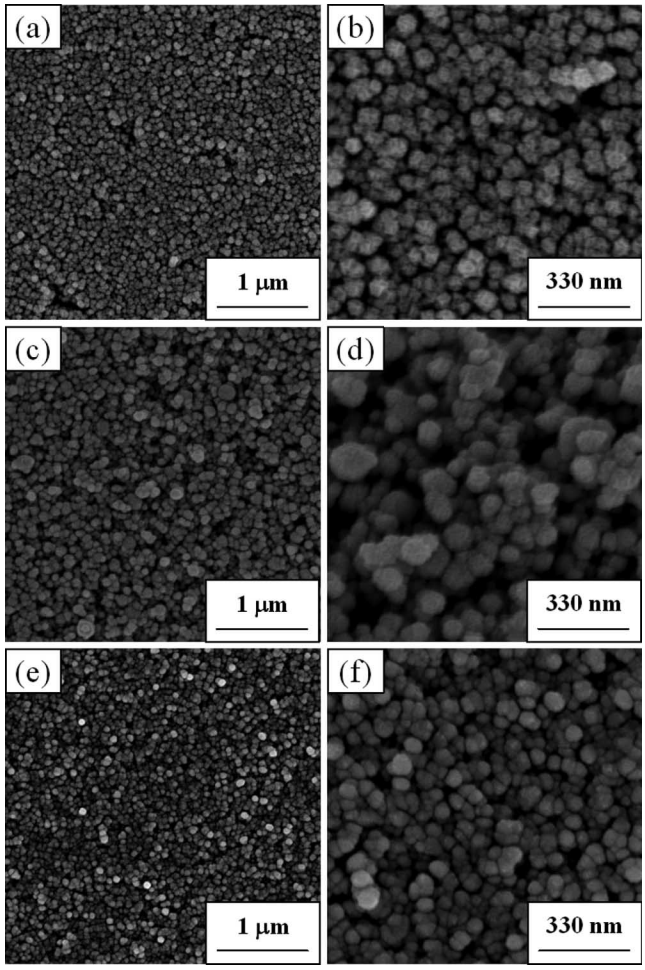

Fig. 4. SEM images of doctor-bladed TiO_2 films prepared from (a) and (b) FSP-3, (c) and (d) FSP-5, and (e) and (f) commercial benchmark Nanoxide-T.

to almost unchanged (22 to 19 $m^2 \cdot g^{-1}$) for FSP-5 (see Table I). The observation augurs well with the thermal stability of the sintering-induced aerosol growth within the flame, where the lowest rate of combustion enthalpy coupled with rapid quenching in the open-flame configuration renders the lowest flame temperature and residence time for FSP-1, whereas the opposite is true for FSP-5. The decrease in SSA of TiO_2 upon film calcination and the absence of signifcant crystal growth (see Table I) is indicative of the interparticle necking. On the other hand, the sintering and necking of Nanoxide-T crystal is evident from the particle size growth (d_A from 13 to 21 nm) in tandem with the significant decrease in SSA from 120 to 62 $m^2 \cdot g^{-1}$.

B. Electron Diffusion Coefficient (D), Electron Lifetime (τ), Open-Circuit Voltage (V_{oc}), and Capacitance (C) Measurements

The results of D, τ , V_{oc}, and C for DSSCs based on all FSP TiO_2 nanoparticles and commercial TiO_2 materials are shown in Fig. 6. The observed trends of increasing D [see Fig. 6(a)] and decreasing τ [see Fig. 6(b)] with increasing light intensity have been earlier attributed to the filling of charge traps by photoinjected electrons [22]–[25]. On the basis of a multiple trapping model, measured D values are in effect apparent

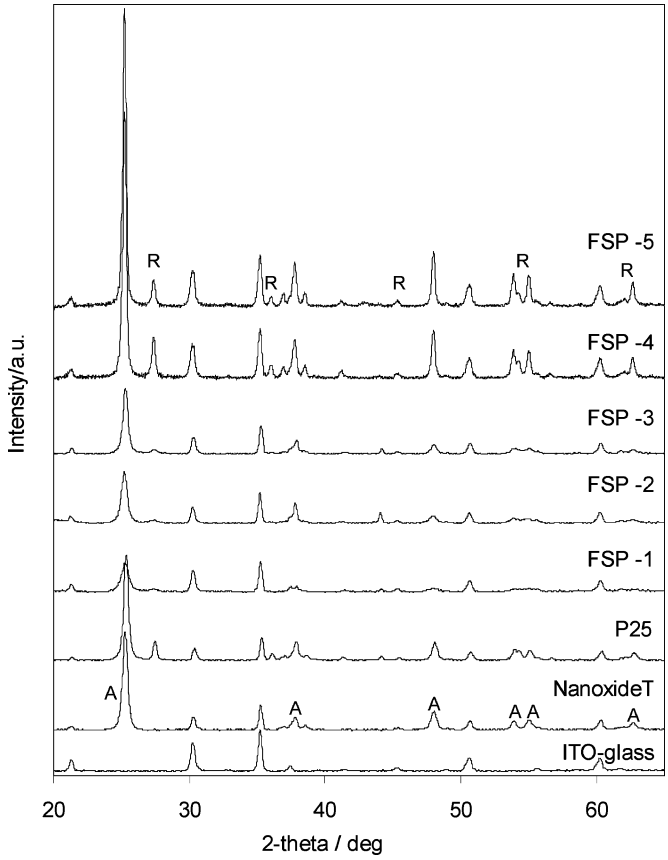

Fig. 5. XRD spectra of doctor-bladed TiO_2 particulate films on conductive indium tin oxide glass, fabricated from FSP samples, as well as Degussa P25 and Nanoxide-T. The characteristics peaks of anatase are labeled "A," while those of rutile are labeled "R."

values, reflecting diffusion time and time spent in traps. Transport-limited recombination also takes into account time spent on the TiO_2 conduction band and time to transfer through TiO_2/dye/electrolyte interfaces. Regarding DSSCs based on FSP TiO_2, D increased with decreasing SSA. The higher content of surface and boundary defects for high SSA particles, given their shorter residence time and lower flame temperature during synthesis, resulted in increased trapping of electrons within the TiO_2 particulate film. This was further corroborated by the shorter observed τ as SSA decreased, consistent with the transport-limited recombination model. In other words, a relatively high density of interband traps limited diffusion, but at the same time prolonged lifetime. A higher density of interband charge traps with increasing SSA was also suggested from Fig. 6(c). Fig. 6(c) provides the relationship between the Fermi level (E_F) of the TiO_2 electrodes as a function of electron density. Assuming that the conduction-band edge potential ($E_{\rm CB}$) is the same among the samples, the difference in E_F at matched electron density originates from the difference in the trap density and distribution. Since the slope of the plot gives the capacitance ($dV/dQ = 1/C$), which is related to traps, the plot suggests higher trap densities for higher SSA films (e.g., 0.87 mF·cm^{-2} around 0.72 V for FSP-3, and 0.24 mF·cm^{-2} around 0.70 V for FSP-4). Note that a very similar $E_{\rm CB}$ is implied from the short-circuit current of the solar cells.

The aforementioned relationship between SSA and the density of interband charge traps was further confirmed by direct measurements of C as a function of V in Fig. 6(d), which shows lower trap density and its steeper distribution for higher SSA films (FSP-4 and FSP-5) in comparison to lower SSA films (FSP-3). When the capacitances were normalized to SSA, the values of FSP-4 and FSP-5 appeared to be lower than that of FSP-3. This further points to the difference between particles synthesized in the enclosed and open flame, beyond a pure function of size. Compared to the rapid quenching in the open flame, the more intense time–temperature profile within the enclosed flame provided sufficient heat and time for the healing of intrinsic defects [21]. It has been earlier suggested that electron traps are located at the particle surface with similar surface trap density. This was derived from an analysis showing that electron trap density was proportional to the surface area of the films [26]. If the surface trap density for FSP-4 and FSP-5 was indeed lower, the FSP method could in principle be used to control the surface trap density independently from the particle size. However, based on the data shown in Fig. 6, we cannot rule out the possibility that the particle size influences the trap density by mechanisms other than the aforementioned surface area effect.

C. Comparison to Commercially Available TiO_2 Particles

Considering commercial materials, the D and τ values observed for P25 (see Fig. 6) fell in qualitative agreement with the general trends in D and τ observed for FSP TiO_2 nanoparticles. This is unsurprising, since these materials were all flame-made, even though there are subtle differences in properties between these two otherwise different types of flame syntheses. For example, while the data of P25 in Fig. 6(c) is almost identical to that of FSP-2, there exists a higher surface trap density in P25 due to its lower SSA. This may be attributed to the lower flame synthesis temperature, which uses the oxyhydrogen flame as fuel source [19] as compared to the oxyhydrocarbon (xylene/CH_3CN) flame in FSP. As for the case of Nanoxide-T, the D and τ values did not appear to follow these trends. Among the samples in Fig. 6(c), Nanoxide-T showed one of the lowest $V_{\rm oc}$ values at matched electron density. This suggested high surface trap density, consistent with the observed comparatively long τ value. According to the trap-controlled transport model, high trap density generally results in low values of D. The high D values of Nanoxide-T samples in Fig. 6(a) can be explained by the different degree of interparticle hopping rate, which is related to the degree of neck growth between particles as reported earlier [3], and also reflected by the significant loss in SSA after film fabrication. The ability of better necking of particles synthesized via the low-temperature hydrothermal method appears to be an advantage; however, the associated higher trap density is clearly a drawback.

D. Implications for DSSCs

Fig. 7 compares the current density–voltage (I–V) curves of DSSCs based on FSP TiO_2 particles and commercial TiO_2. The

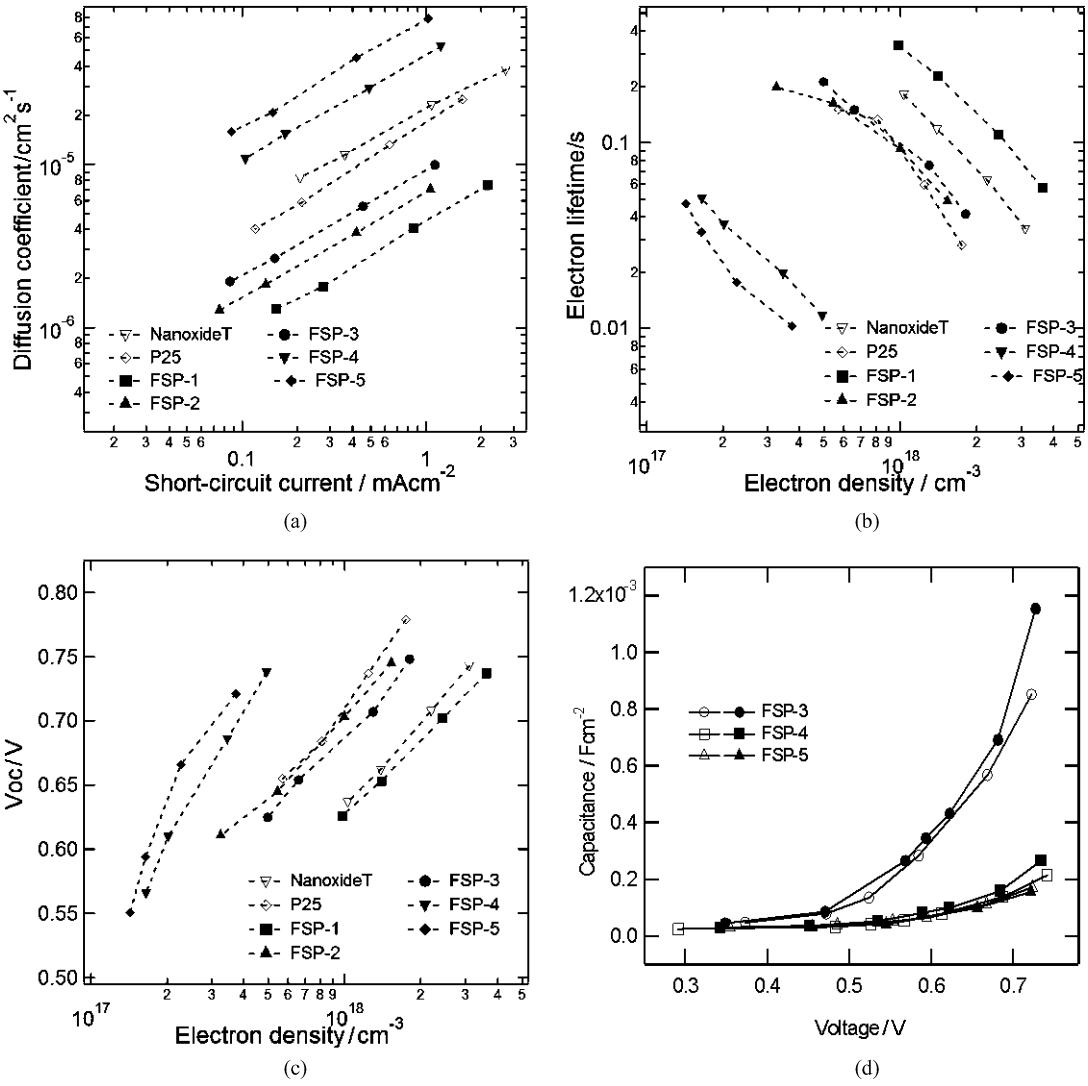

Fig. 6. (a) Electron diffusion coefficient (D), (b) electron lifetime (τ), (c) open-circuit voltage ($V_{\rm oc}$), and (d) capacitance (C) of DSSCs. For (d), data from two identical samples are shown.

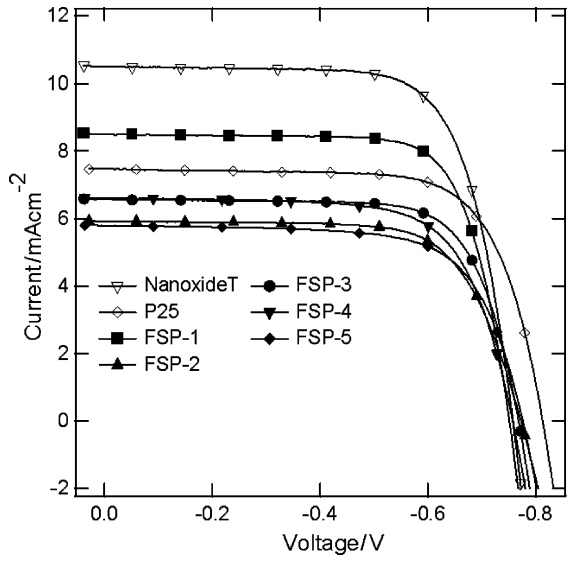

Fig. 7. *I–V* characteristics of DSSCs under one-sun conditions. Thickness of the TiO_2 electrodes was 5–6 μm.

I–V curves of the same devices used for SLIM-PCV studies are shown. DSSCs based on FSP-4 and FSP-5 showed relatively high $V_{\rm oc}$ despite low short-circuit current ($J_{\rm sc}$) values. This was somewhat unexpected due to their very short electron lifetime. The $V_{\rm oc}$ is determined by the electrochemical potential, where the electrons are located at open-circuit conditions, which is determined not only by the electron density, but also the concentration and the energy distribution of the traps. Although the electron density was low (given by $G \times \tau$, where G is the charge generation rate), due to the lower charge trap concentration for FSP-4 and FSP-5, more traps were filled and a large proportion of electrons were located at more negative potential, closer to the $E_{\rm CB}$. This resulted in more negative E_F for these DSSCs. This shows important implications to design TiO_2 nanoparticles for high-performance DSSCs: the $V_{\rm oc}$ can be increased by reducing the concentration of charge traps, although τ is substantially shortened. This is also supported by the observed low $V_{\rm oc}$ of the DSSC based on Nanoxide-T together with long τ under one-sun conditions.

In terms of J_{sc}, all DSSCs based on FSP TiO_2 particles showed lower values compared to the DSSC based on Nanoxide-T. In the case of the DSSC based on FSP-3, the J_{sc} value increased at least up to 20 μm film thickness (data not shown), which indicated that the diffusion length did not limit J_{sc}. The amount of dye uptake was also found to be similar among samples. Thus, it is possible that initial charge separation may have limited the J_{sc} of DSSCs based on these FSP particles. Interestingly, the DSSC based on P25 showed relatively high J_{sc} values. The main difference between P25 and FSP was suggested earlier to be in their relative surface trap densities [see Fig. 6(c)]. This could imply that charge traps may be required to hold the injected electrons until the dye cation is reduced by I^-. If so, $TiCl_4$ treatment, which is known to increase the injection yield, would likely lead to an increase in J_{sc} [27]. In addition, particle size dependent charge injection has been reported earlier [28], and this might have been applicable to the FSP TiO_2 samples considered here, which generally demonstrated larger particle sizes than optimal for DSSCs. A detailed injection study is beyond the scope of this paper, while it should be clarified in further experiments to develop a complete understanding of the fundamental requirements for synthesizing TiO_2 electrodes for high-performance DSSCs.

IV. Conclusion

FSP synthesis via open- and enclosed-flame methods was employed to prepare various sizes of TiO_2 nanoparticles. Mirrored trends in the charge-transport parameters D and τ suggested that interband charge trap density decreased with increasing FSP TiO_2 nanoparticle size, and this was confirmed by separate C measurements and the slope of V_{oc} versus electron density plots. Despite the significantly shorter τ observed for larger TiO_2 particles, the corresponding V_{oc} of DSSCs under one-sun conditions was relatively high. This showed that V_{oc} can be increased by decreasing trap density. The different surface trap densities estimated for open-flame and enclosed-flame TiO_2 demonstrated that the FSP process can be tuned so that charge-transport properties are controlled somewhat independently of particle size. In comparison to commercially available TiO_2 particles, no disadvantage of electron-transport properties and higher open-circuit voltage were found.

Acknowledgment

The authors would like to thank D. Li (UNSW) for part of the TEM imaging and G. Triani from the Australian Nuclear Science and Technology Organization for provision of TiO_2 paste formulation method.

References

[1] B. C. O'Regan and M. Grätzel, "A low-cost, high-efficiency solar cell based on dye-sensitized colloidal titanium dioxide films," *Nature*, vol. 353, pp. 737–740, 1991.

[2] Y. Cao, Y. Bai, Q. Yu, Y. Cheng, S. Liu, D. Shi, F. Gao, and P. Wang, "Dye-sensitized solar cells with a high absorptivity ruthenium sensitizer featuring a 2-(Hexylthio)thiophene conjugated bipyridine," *J. Phys. Chem. C*, vol. 113, pp. 6290–6297, 2009.

[3] S. Nakade, M. Matsuda, S. Kambe, Y. Saito, T. Kitamura, T. Sakata, Y. Wada, H. Mori, and S. Yanagida, "Dependence of TiO_2 nanoparticle preparation methods and annealing temperature on the efficiency of dye-sensitized solar cells," *J. Phys. Chem. B*, vol. 106, pp. 10004–10010, 2002.

[4] S. Ito, P. Chen, P. Comte, M. K. Nazeeruddin, P. Liksa, P. Pechy, and M. Gräzel, "Fabrication of screen-printing pastes from TiO_2 powders for dye-sensitised solar cells," *Prog. Photovoltaics Res. Appl.*, vol. 15, pp. 603–612, 2007.

[5] R. Strobel and S. E. Pratsinis, "Flame aerosol synthesis of smart nanostructured materials," *J. Mater. Chem.*, vol. 17, pp. 4743–4756, 2007.

[6] W. Y. Teoh, R. Amal, and L. Mädler, "Inter-relationship between Pt oxidation states on TiO_2 and the photocatalytic mineralisation of organic matters," *J. Catal.*, vol. 251, pp. 271–280, 2007.

[7] W. Y. Teoh, R. Amal, L. Mädler, and S. E. Pratsinis, "Flame sprayed visible light-active Fe-TiO_2 for photomineralisation of oxalic acid," *Catal. Today*, vol. 120, pp. 203–213, 2007.

[8] W. Y. Teoh, F. Denny, R. Amal, D. Friedmann, L. Mädler, and S. E. Pratsinis, "Photocatalytic mineralisation of organic compounds: A comparison of flame-made TiO_2 catalysts," *Top. Catal.*, vol. 44, pp. 489–497, 2007.

[9] W. Y. Teoh, L. Mädler, D. Beydoun, S. E. Pratsinis, and R. Amal, "Direct (one-step) synthesis of TiO_2 and Pt/TiO_2 nanoparticles for photocatalytic mineralisation of sucrose," *Chem. Eng. Sci.*, vol. 60, pp. 5852–5861, 2005.

[10] T. Kanzaki, S. Nakade, Y. Wada, and S. Yanagida, "Retardation of interfacial charge recombination by addition of quaternary ammonium cation and its application to low temperature processed dye-sensitzed solar cells," *Photochem. Photobiol. Sci.*, vol. 5, pp. 389–394, 2006.

[11] R. W. Cheary and A. Coelho, "A fundamental parameters approach to X-ray line-profile fitting," *J. Appl. Cryst.*, vol. 25, pp. 109–121, 1992.

[12] S. Nakade, T. Kanzaki, Y. Wada, and S. Yanagida, "Stepped light-induced transient measurements of photocurrent and voltage in dye-sensitized solar cells: Application for highly viscous electrolyte systems," *Langmuir*, vol. 21, pp. 10803–10807, 2005.

[13] N. W. Duffy, L. M. Peter, R. M. G. Rajapakse, and K. G. U. Wijayantha, "A novel charge extraction method for the study of electron transport and interfacial transfer in dye sensitised nanocrystalline solar cells," *Electrochem. Commun.*, vol. 2, pp. 658–662, 2000.

[14] S. Nakade, T. Kanzaki, W. Kubo, T. Kitamura, Y. Wada, and S. Yanagida, "Role of electrolytes on charge recombination in dye-sensitized TiO_2 solar cell (1): The case of solar cells using the I^-/I_3^- redox couple," *J. Phys. Chem. B*, vol. 109, pp. 3480–3487, 2005.

[15] S. Nakade, Y. Saito, W. Kubo, T. Kanzaki, T. Kitamura, Y. Wada, and S. Yanagida, "Enhancement of electron transport in nano-porous TiO_2 electrodes by dye adsorption," *Electrochem. Commun.*, vol. 5, pp. 804–808, 2003.

[16] B. C. O'Regan, K. Bakker, J. Kroeze, H. Smit, P. M. Sommeling, and J. R. Durrant, "Measuring charge transport from transient photovoltage rise times. A new tool to investigate electron transport in nanoparticle films," *J. Phys. Chem. B*, vol. 110, pp. 17155–17160, 2006.

[17] B. C. O'Regan and J. R. Durrant, "Calculation of activation energies for transport and recombination in mesoporous TiO_2/dye/electrolyte films taking into account surface charge shifts with temperature," *J. Phys. Chem. B*, vol. 110, pp. 8544–8547, 2006.

[18] H. Schulz, L. Mädler, S. E. Pratsinis, P. Burtscher, and N. Moszner, "Transparent nanocomposites of radiopaque flame-made Ta_2O_5/SiO_2 particles in an acrylic matrix," *Adv. Funct. Mater.*, vol. 15, pp. 830–837, 2005.

[19] S. E. Pratsinis, "Flame aerosol synthesis of ceramic powders," *Prog. Energy Combust. Sci.*, vol. 24, pp. 197–219, 1998.

[20] A. Teleki, N. Bjelobrk, and S. E. Pratsinis, "Flame-made Nb- and Cu-doped TiO_2 sensors for CO and ethanol," *Sens. Actuat B-Chem.*, vol. 130, pp. 449–457, 2008.

[21] D. Li, W. Y. Teoh, R. C. Woodward, J. D. Cashion, C. Selomulya, and R. Amal, "Evolution of morphology and magnetic properties in silica/maghemite nanocomposites," *J. Phys. Chem. C*, vol. 113, pp. 12040–12047, 2009.

[22] J. Bisquert, A. Zaban, M. Greenshtein, and I. Mora-Sero, "Determination of rate constants for charge transfer and the distribution of semiconductor and electrolyte electronic energy levels in dye-sensitized solar cells by open-circuit photovoltage decay method," *J. Amer. Chem. Soc.*, vol. 126, pp. 13550–13559, 2004.

[23] N. Kopidakis, K. D. Benkstein, J. van de Lagemaat, and A. J. Frank, "Transport-limited recombination of photocarriers in dye-sensitized nanocrystalline TiO_2 solar cells," *J. Phys. Chem. B*, vol. 107, pp. 11307–11315, 2003.

[24] J. Nelson, "Continuous-time random-walk model of electron transport in nanocrystalline TiO_2 electrodes," *Phys. Rev. B*, vol. 59, pp. 15374–15380, 1999.
[25] N. G. Park, J. van de Lagemaat, and A. J. Frank, "Comparison of dye-sensitized rutile- and anatase-based TiO_2 solar cells," *J. Phys. Chem. B*, vol. 104, pp. 8989–8994, 2000.
[26] N. Kopidakis, N. R. Neale, K. Zhu, J. van de Lagemaat, and A. J. Frank, "Spatial location of transport-limiting traps in TiO_2 nanoparticle films in dye-sensitized solar cells," *Appl. Phys. Lett.*, vol. 87, pp. 202106–202108, 2005.
[27] B. C. O'Regan, J. R. Durrant, P. M. Sommeling, and N. J. Bakker, "Influence of the $TiCl_4$ treatment on nanocrystalline TiO_2 films in dye-sensitized solar cells. 2. Charge density, band edge shifts, and quantification of recombination losses at short circuit," *J. Phys. Chem. C*, vol. 111, pp. 14001–14010, 2007.
[28] G. Benko, B. Skarman, R. Wallenburg, A. Hagfeldt, V. Sundstrom, and A. K. Yartsev, "Particle size and crystallinity dependent electron injection in fluorescein 27-sensitized TiO_2 films," *J. Phys. Chem. B*, vol. 107, pp. 1370–1375, 2003.

George Tsekouras received the B.Sc. (Hons.) and Ph.D. degrees from the University of Wollongong, Wollongong, N.S.W., Australia, in 2002 and 2005, respectively.

He was a Postdoctoral Research Fellow at the University of Wollongong, during 2005–2007 and at Uppsala University, Sweden, during 2008. He is currently a Research Fellow at the University of St. Andrews, Fife, U.K. His research interests include the utilization of new ceramics for high-temperature steam electrolysis, while his previous research interests included dye-sensitized solar cells and molecular electronics.

Masanori Miyashita received the B.Eng. and M. Chem. Eng. degrees from Shinshu University, Matsumoto, Nagano, Japan, in 2007 and 2009, respectively.

He is currently an Engineer at Toray Industries, Inc., Tokyo, Japan.

Yung Kent Kho received the B.E. (Hons.) degree in chemical engineering in 2006 from The University of New South Wales, Sydney, Australia, where she is currently working toward the Doctorate degree in chemical engineering.

Her research interest includes the flame synthesis of nanoparticles and their further adaptation in clean energy applications, including dye-sensitized solar cells and solar water splitting.

Wey Yang Teoh received the B.E. (Hons.) degree in chemical engineering, and the Ph.D. degree from The University of New South Wales, Sydney, Australia, in 2003 and 2007, respectively.

He is an ARC Australian Postdoctoral Fellow (APD). His research interests include the design and fabrication of functional nanoparticles by flame spray pyrolysis. He will assume the position of Assistant Professor at the School of Energy and Environment, City University of Hong Kong, Shatin, Hong Kong.

Attila Janos Mozer received the Ph.D. degree in physical chemistry from the Linz Institute for Organic Solar Cells, Johannes Kepler University Linz, Linz, Austria.

He is a Senior Fellow and the Team Leader for solar energy conversion at the Intelligent Polymer Research Institute and the Australian Research Council Center of Excellence for Electromaterials Science, Intelligent Polymer Research Institute, University of Wollongong, N.S.W., Australia. He was involved in developing solid-state dye-sensitized solar cells at Osaka University, Japan with Prof. S. Yanagida. His research interests include the main areas of organic solar cell research including polymer bulk-heterojunction solar cells, solid and liquid dye-sensitized solar cells, specializing in time-resolved spectroscopic measurements of charge transport, and recombination in these solar cell materials and devices.

Dr. Mozer received a Postdoctoral Fellowship from the Japanese Society for the Promotion for Science in 2005.

Rose Amal received the Ph.D. degree in chemical engineering from The University of New South Wales (UNSW), Sydney, Australia, in 1991.

She is an Australian Research Council (ARC) Australian Professorial Fellow (APF) and a Scientia Professor at the UNSW, where she is the Head of the Particles and Catalysis Research Group, School of Chemical Engineering, and has been involved in graduating more than 20 doctorate students. She was the Co-Director of the ARC Center of Excellence for Functional Nanomaterials during 2005, and the Director of the multi-institution research center during 2009 to present. She is also the Inaugural Director of the Center for Energy Research and Policy Analysis, Energy Research Institute, UNSW. Her research interests include particles technology and nanomaterials, spreading over a wide range of applications from energy, environmental to bioapplications.

Shogo Mori received the B.S. and M.S. degrees in physics from the University of Toledo, Toledo, OH, in 1996 and 1998, respectively, and the Ph.D. degree in engineering science from Osaka University, Osaka, Japan, in 2004.

Since 2005, he has been with the Faculty of Textile Science and Technology, Shinshu University, Nagano, Japan, where he is currently an Associate Professor. His research interests include interactions between photon and materials, and charge transport and transfer, especially at semiconductor/dye/electrolyte interface in dye-sensitized solar cells.

Gordon G. Wallace received the Ph.D. degree from Deakin University, Geelong, Australia, in 1983.

He joined the University of Wollongong, N.S.W., Australia, in 1986, where he is currently the Director of the Intelligent Polymer Research Institute and the Executive Research Director of the Australian Research Council Center of Excellence for Electromaterials Science. He has authored or coauthored more than 500 papers and numerous patents on organic conductors, nanomaterials, the development of intelligent polymer systems, and their exploitation in medical bionics and energy production and storage.

Dr. Wallace is a Fellow of the Australian Academy of Science and the Australian Academy of Technological Sciences and Engineering.